

**Manuscript version: Author's Accepted Manuscript**

The version presented in WRAP is the author's accepted manuscript and may differ from the published version or Version of Record.

**Persistent WRAP URL:**

<http://wrap.warwick.ac.uk/128455>

**How to cite:**

Please refer to published version for the most recent bibliographic citation information. If a published version is known of, the repository item page linked to above, will contain details on accessing it.

**Copyright and reuse:**

The Warwick Research Archive Portal (WRAP) makes this work by researchers of the University of Warwick available open access under the following conditions.

Copyright © and all moral rights to the version of the paper presented here belong to the individual author(s) and/or other copyright owners. To the extent reasonable and practicable the material made available in WRAP has been checked for eligibility before being made available.

Copies of full items can be used for personal research or study, educational, or not-for-profit purposes without prior permission or charge. Provided that the authors, title and full bibliographic details are credited, a hyperlink and/or URL is given for the original metadata page and the content is not changed in any way.

**Publisher's statement:**

Please refer to the repository item page, publisher's statement section, for further information.

For more information, please contact the WRAP Team at: [wrap@warwick.ac.uk](mailto:wrap@warwick.ac.uk).

# Effects of the die parameters on the self-piercing riveting process

Yunpeng Liu<sup>1</sup>, Han Li<sup>2</sup>, Huan Zhao<sup>1</sup> and Xianping Liu<sup>1\*</sup>

<sup>1</sup>School of Engineering, University of Warwick, Coventry CV4 7AL, UK

<sup>2</sup>Jaguar Land Rover, Coventry CV3 4LF, UK

\*X.Liu@warwick.ac.uk

## Abstract:

To facilitate the die selection for new self-piercing riveting (SPR) joint configurations, it is necessary to find out how the critical die geometric parameters influence the SPR process. In this study, a two-dimensional (2D) axisymmetric simulation model was developed to numerically study the riveting process. The influences of the die type, the die diameter, the die depth and the die pip height on the deformation behaviour of the rivet and sheets were systematically studied. Moreover, the flared rivet shank radius and the thickness at the centre of the bottom sheet during the SPR process were first monitored using the developed simulation model. The simulation results revealed that these die parameters have significant influences on the deformation behaviour of the rivet and sheets. The flared rivet shank radius showed an increasing trend with the increment of the die diameter and the die pip height, while it decreased with the increment of the die depth. Furthermore, it was also found that the flaring speed of the rivet shank depended heavily on the filling condition of the die cavity underneath the rivet cavity. A rapid flare of the rivet shank was observed when this space was fully filled.

**Keywords:** self-piercing riveting; die geometries; die type; material deformation; FEM

## 1 Introduction

Nowadays, lightweight materials, such as aluminium alloys and composites, have been widely used in the automotive industry. Resistance spot welding (RSW) technique is the most popular joining method to assemble steel parts in the car industry, but it is not suitable for dissimilar materials due to the different material properties [1-2]. As an alternative, SPR technique is now widely adopted in the car body-in-white (BIW) assembly process [3-4]. SPR is a mechanical joining process relying on the rivet and die to form a sufficient mechanical connection between the rivet shank and the bottom sheet. It has many advantages, such as the capability to join dissimilar materials, no requirement for the surface conditions and environment friendly (no fume, no spark and low noise) [5-6].

To form sufficient mechanical connection, the rivet and sheets, especially the bottom sheet, always undergo very large plastic deformations during the SPR process. The die plays a significant role during the riveting process as its main function is to guide the deformations of the rivet and sheets. The die geometry can therefore significantly affect the joint quality, in terms of the interlock, the minimum remaining thickness of the bottom sheet and the rivet head height. Many studies have been carried out to investigate the influences of the die parameters on the SPR process and the joint quality. For instance, Li et al. [7] experimentally found that the die profile had significant effects on the joint quality, mechanical strengths and failure behaviour. Ma et al. [8] experimentally investigated the influence of the die diameter and the die pip height on the rivetability of the AA6061-T6 and mild steel CR4 sheets. It was discovered that the changes of the die diameter and pip height mainly influenced the deformation behaviour of the sheets, and thus led to the change of the joint quality. Mori et al. [9] numerically optimized the die profile for SPR joint with high strength steel and aluminium alloy sheets using finite element method (FEM). It was found that the severe compression of the rivet leg when piercing the top high strength steel sheet could be eliminated by optimizing

the die diameter and depth. Similarly, Abe et al. [10] numerically optimized the die profile and discovered that the die with larger depth and diameter could effectively extend the joining range of the three layer joints with different high strength steels.

In addition, with a 2D simulation model in DEFORM, Mathias et al. [11] studied the effects of the die geometric parameters on the SPR joint quality and found that the die depth was the most significant die parameter. A novel die geometry with a moveable bottom was proposed in their paper to compensate the changes of the boundary conditions, and thus led to a consistent joint quality. Similarly, a die with a force-controlled moveable bottom was proposed and numerically studied by Drossel and Jackel [12] to improve the joinability of materials with limited ductility using SPR. It was found that the force-controlled moveable die bottom could apply a pressure on the bottom sheet, and superimpose compressive stresses on the riveting zone to prevent the appearance of cracks on the bottom sheet. Landgrebe et al. [13] experimentally studied the damages of the carbon fibre reinforced plastic (CFRP) sheet during SPR process, and compared the effects of the traditional die and the new die with a moveable bottom proposed by Drossel and Jackel [12]. Less delamination but more fibre or matrix fractures in the CFRP sheet were captured with the new moveable die compared with that with conventional die. Hoang et al. [14] numerically and experimentally studied the effects of the die type (flat die and pip die) on the SPR joint with aluminium sheets and aluminium rivet. The results revealed that the die profile had a crucial influence on the joint quality and the fracture of the bottom.

Although the influences of the die geometries on the SPR joint have been widely investigated over the last few decades, most of these studies paid more attentions to the joint quality rather than the SPR process. Meanwhile, most of the conclusions in these studies were made by analysing the final joint cross-sectional profiles. However, the deformation behaviour of the rivet and sheets during the joining process directly affects the magnitudes of the interlock, the minimum remaining thickness of the bottom sheet and the rivet head height. The parameter changes of the die, whose main function is to guide the deformation of the rivet and sheets, would inevitably influence the deformation behaviour of the rivet and sheets. Therefore, it is necessary to find out how the die parameters affect the deformations of the rivet and sheets, and how the material deformation affect the formation of the critical joint quality indicators. A deeper understanding of the SPR processes with different dies would be helpful to form guidelines of how to select a suitable die for a given sheets combination, and how to develop new type dies. These guidelines are urgently required in the automotive industry to broaden the applications of the SPR technique.

This study systematically investigated the influences of the die parameters, including the type, diameter, depth and pip height, on the deformation behaviour of the rivet and sheets with a 2D axisymmetric SPR simulation model. Meanwhile, the rivet shank flaring behaviour and the thinning process of the bottom sheet were numerically recorded and analysed for the first time. The relationships between the material deformations and the SPR joint quality were also discussed. Compared with the experimental test, the finite element method demonstrated huge advantages in efficiency for understanding the SPR process.

## 1.1 Establishment of the simulation model

Due to the axisymmetric property of the SPR joint, axisymmetric deformations of the rivet and sheets were assumed. The software Simufact.Forming was used to develop the 2D simulation model. In order to shorten the simulation time, only the parts around the joining region were modelled as shown in Fig. 1. Six parts were involved in the model: (1) punch; (2) blank-holder; (3) die; (4) rivet; (5) top sheet and (6) bottom sheet. The blank-holder, punch and die were modelled as rigid bodies, while the rivet, top and bottom sheets were modelled as elastic-plastic bodies.

The rivet was meshed using 4-nodes quadtree elements with four gauss points to allocate more elements on the rivet surface, while the top and bottom sheets were meshed using 4-nodes advancing front quad elements

to get uniform elements. A mesh sensitivity study was carried out to find suitable mesh sizes for the rivet and sheets. In this model, the mesh sizes for the rivet, top sheet and bottom sheet were 0.10 mm, 0.10 mm and 0.12 mm respectively. As presented in **Fig. 1**, mesh refinement boxes were applied on the rivet tip (red box) and the central areas of the two sheets (yellow and green boxes). This can distribute fine meshes around the joining region in the initial mesh, and improve the prediction accuracy without increasing too much simulation time. During the SPR process, the top and bottom sheets undergo severe plastic deformations, which can cause serious mesh distortion and convergence problems during the simulation [15]. To deal with this issue, the automatic re-meshing technique based on different re-meshing criteria was adopted for the top and bottom sheets. The re-meshing criteria for the top sheet are element distortion criterion, strain change criterion and minimum thickness criterion. While the re-meshing criteria for the bottom sheet are only element distortion criterion and strain change criterion. The minimum thickness criterion works together with a geometrical criterion to model the blanking of the top sheet. As for the rivet, the material deformation is not very large and the initial rivet mesh is fine enough to avoid severe element distortion as well as the convergence problems. Thus, the re-meshing technique was not used for the rivet.

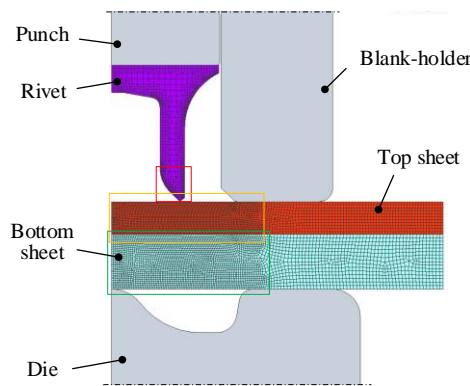


**Fig. 1** Schematic of the SPR simulation model

The materials of the two sheets and the rivet are AA5754 aluminium alloy and boron steel respectively. The mechanical properties of these two materials are listed in **Table 1**. Plastic stress-strain curves were utilized to describe the deformations of the rivet and sheets during the riveting process. The stress-strain curves of AA5754 aluminium alloy were provided by Jaguar Land Rover (JLR) and described in details by Mario et al. [16], in which the thermal softening effect and strain rate hardening effect were considered. However, due to the high punch velocity (100 mm/s), the sheet material deformed under very large strain rates (above  $100 \text{ s}^{-1}$ ) during the riveting process. The stress-strain curves obtained under low level strain rates ( $0.01$ ,  $0.1$  and  $1 \text{ s}^{-1}$ ) are incapable of modelling the strain rate hardening effect on the material. Therefore, the strain rate hardening effect on the sheet material was not considered, and only the stress-strain curves under the highest strain rate ( $1 \text{ s}^{-1}$ ) were employed as shown in **Fig. 2**. Meanwhile, the thermal softening effect has a significant influence on the sheet material properties and was considered in this model. The stress-strain curve (strain rate= $0.01 \text{ s}^{-1}$ ) of boron steel provided by JLR was used to describe the deformation of the rivet as shown in **Fig. 3**. During the SPR process, the maximum temperature within the joining region is lower than  $250^\circ\text{C}$  [17], which has very limited influence on the mechanical properties of the boron steel. So the thermal effect on the rivet material was not considered.

**Table 1** Material properties of the rivet and sheets

Material	Young's Modules (GPa)	Poisson's ratio
AA5754	70	0.3
Boron steel	200	0.3

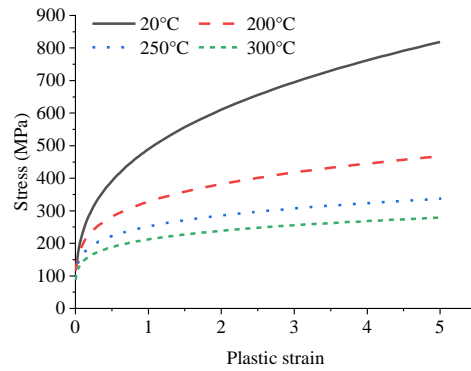


**Fig. 2** Plastic stress-strain curves of AA5754 (strain rate=1 s<sup>-1</sup>) [17]

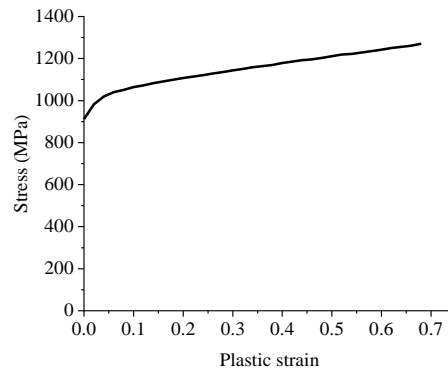


**Fig. 3** Plastic stress-strain curve of the boron steel (strain rate=0.01 s<sup>-1</sup>)

To model the blanking of the top sheet, a geometrical criterion, which defines the occurrence of blanking once the top sheet thickness reduces to the predefined critical value, was implemented in the simulation model. The critical thickness, as shown in Fig. 4, used in the geometrical criterion has a significant influence on the predicted joint quality, especially the interlock. In general, with the decrease of the material ductility, the blanking of the top sheet would occur at an earlier time and a larger critical thickness should be used. However, too large critical thickness could lead to a premature fracture of the top sheet, while too small critical thickness could cause an unrealistic deformation of the top sheet material around the fracture location. By comparing final shapes of the rivet and sheets on the cross-sectional profiles from the simulations and experiments, it was found that the suitable critical thickness for the AA5754 top sheet was 0.04 mm. By analysing all the experiment data of SPR joints from JLR, it was found that the rivet and bottom sheet fracture was only observed in a few joints involving high strength steels or brittle materials as the bottom sheet material. In this study, the bottom sheet was made of high ductile material AA5754. Hence to simplify the simulation model, it was assumed that no fracture of the rivet and bottom sheet would happen under the joint configurations used in this study.

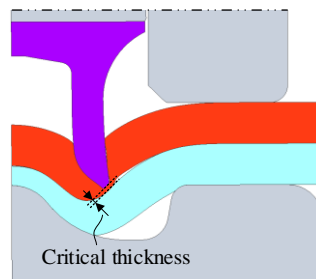


**Fig. 4** The critical thickness for the blanking of the top sheet

The **Coulomb** friction model was chosen to describe the interactions between the contacted surfaces. The friction coefficients between different surfaces have a significant influence on the deformation behaviour of the rivet and sheets [18]. For instance, the friction coefficient between the bottom sheet and the die could directly affect the final thickness distribution of the bottom sheet, while the friction coefficient between the top sheet and the rivet could directly influence the rivet shank flaring distance [19-20]. **Therefore, the inverse method, by comparing the final shapes of the rivet and sheets from the simulations and experiments, was used to determine the friction coefficients between different interfaces.** In this model, it was found that the suitable friction coefficient between the bottom sheet and the die was 0.22, while the suitable friction coefficient between other parts was 0.10. The clamping force between the die and blank-holder is 5.3 kN.

## 1.2 Verification of the simulation model

To verify the proposed simulation model, fourteen SPR joints with different configurations were produced experimentally as listed in **Table 2**. At least three joints for each configuration were made. The cross-sectional profiles of the flat die and the pip die used in the experiment are presented in **Fig. 5**. The cross-sectional profile of the semi-tubular rivet is presented in **Fig. 6**. The punch velocity and clamping force used in the experimental tests are consistent with that used in the simulation.

**Table 2** Joint and die configurations used in the experimental tests

Joint No.	Sheet thickness		Rivet			Die			
	Top sheet (mm)	Bottom sheet (mm)	Radius $R_1$ (mm)	Length $L_1$ (mm)	Hardness	Die type	Depth $H_1$ (mm)	Diameter $D_1$ (mm)	Pip height (mm)
1-1		1.0							
1-2	1.2	1.2	2.65	5.0	H0	Pip	1.6	9.0	0
1-3		1.5							
1-4		2.0							
2-1	1.0								
2-2	1.2	1.5	2.65	5.0	H0	Pip	1.6	9.0	0
2-3	1.5								
3-1		1.2							
3-2	1.5	1.5	2.65	6.0	H0	Pip	1.6	9.0	0
3-3		2.0							
4-1						Pip	1.6	11.5	0
4-2							2.0	8.5	
4-3	1.2	2.0	2.65	5.0	H0	flat	2.0	9.0	--
4-4							1.4	11.0	
4-5							1.6	11.0	

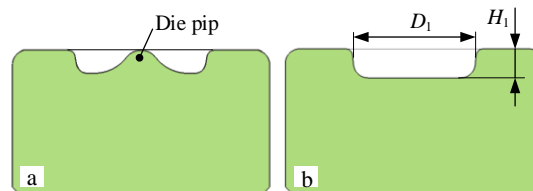


**Fig. 5** Cross-sectional profiles of different type dies: **a** pip die and **b** flat die

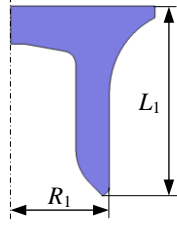


**Fig. 6** Cross-sectional profile of the semi-tubular rivet

All the SPR joints from the experimental tests were sectioned through the centre. Three quality indicators were measured on the joint cross-sectional profile, as shown in **Fig. 7**, to evaluate the SPR joint quality [21], including: (1) the interlock, which is the distance that the rivet shank flared into the bottom sheet along radial direction; (2) the minimum remaining thickness of the bottom sheet ( $T_{\min}$ ), which is the thinnest part of the deformed bottom sheet; and (3) the rivet head height, which is the vertical distance between the top surface of the rivet head and the upper surface of the top sheet. **In the automotive industry, for a sound SPR joint with aluminium alloys sheets and 5.3 mm diameter steel rivet, the interlock should be greater than 0.4 mm, and the  $T_{\min}$  should be no less than 0.2 mm [5]. The rivet head height should be within the range -0.5~+0.3 mm to ensure the surface flatness.** The mean values of these quality indicators were calculated and used for comparison with the simulation results. All the experimental data was provided by JLR.

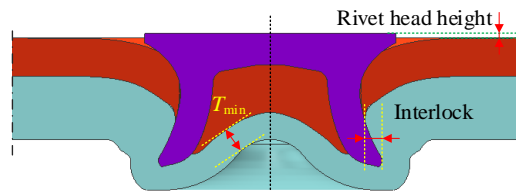


**Fig. 7** Three quality indicators measured on the cross-sectional profile of SPR joint

The rivet head heights obtained from the experimental results were utilized as the termination criterion of the SPR simulations. In other word, the simulation stopped when the simulated rivet head height was equal to the experimental value. Therefore, only the interlock and  $T_{\min}$  were adopted to evaluate the accuracy of the simulation model.

**Fig. 8** and **Fig. 9** present the comparison between the simulation and experimental results of the interlock and  $T_{\min}$ . The Pearson's correlation coefficient ( $r$ ) was adopted to evaluate the prediction accuracy of the simulation model. The calculated values of the  $r$  for the interlock and  $T_{\min}$  are 0.95 and 0.89 respectively, which mean that both of the predicted interlock and  $T_{\min}$  showed a good agreement with that from the experimental tests. Some comparisons of the joint cross-sectional profiles from the simulations and experimental tests are also shown in **Fig. 10**. Similar deformed shapes of the rivet and sheets were observed. Therefore, it is reasonable to believe that the developed simulation model is capable of predicting the cross-sectional profiles during the SPR processes.

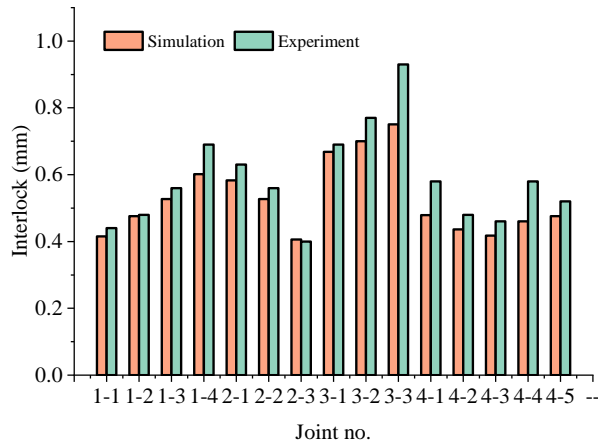


**Fig. 8** Comparison of the interlock values from the experiments and simulations

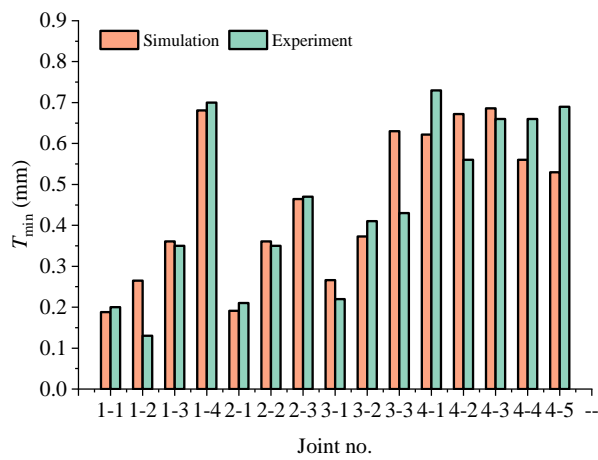


**Fig. 9** Comparison of the minimum remaining thickness on the bottom sheet ( $T_{\min}$ ) from the experiments and simulations

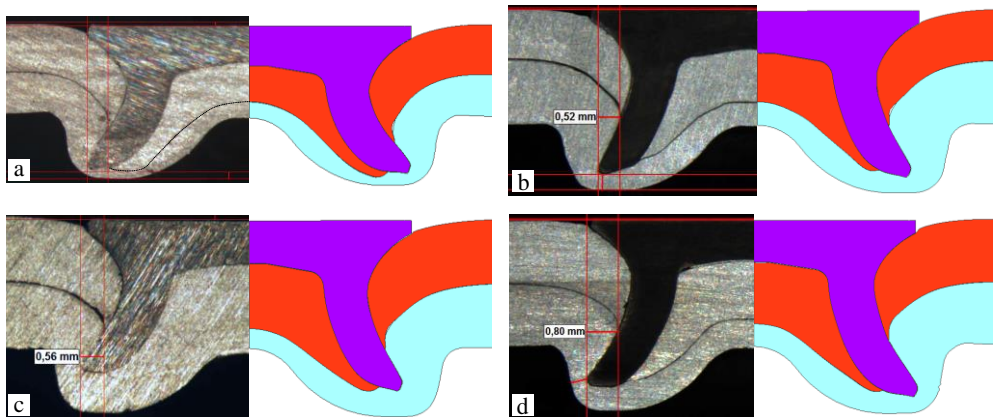


**Fig. 10** Comparison of the joint cross-sectional profiles from the simulations and experimental tests: **a** joint 1-1, **b** joint 1-3, **c** joint 2-3 and **d** joint 3-2

## 2 Influence of the die geometric parameters on the SPR process

The effects of the die geometries, including the die type, the flat die diameter, the flat die depth and the pip height of pip die, on the deformation behaviour of the rivet and sheets were numerically investigated.

### 2.1 Experimental design

The joint configurations used for the study are listed in **Table 3**. Joints 5-1 and 5-2 were simulated to investigate the influence of the die type (flat die and pip die). Joints 5-3, 5-4 and 5-5 made by flat dies with different diameters ranged from 7.5 mm to 14 mm were simulated to study the effects of the die diameter. Joints 5-6 and 5-7 made by flat dies with different die depths were simulated to investigate the die depth effects. Finally, joints 5-8, 5-9 and 5-10 made by pip dies with different pip heights were simulated to discover the influences of the die pip height. The cross-sectional profiles of the pip dies with different die pip heights are illustrated in **Fig. 11**.

**Table 3** Joint configurations with different die geometric parameters

Joint no.	Top sheet thickness (mm)	Bottom sheet thickness (mm)	Rivet		Die				
			Radius $R_1$ (mm)	Length $L_1$ (mm)	Die no.	Die Type	Depth $H_1$ (mm)	Diameter $D_1$ (mm)	Pip height (mm)
5-1	1.2	2.0	2.65	5.0	P1	Pip	1.6	9.0	0
5-2					F1	Flat	2.0	8.5	--
5-3					F2			7.5	
5-4					F3	Flat	2.0	10.0	--
5-5					F4			14.0	
5-6					F5	Flat	1.8	8.5	--
5-7					F6			2.4	
5-8					P1				0
5-9					P2	Pip	1.6	9.0	-0.4
5-10					P3				-0.8

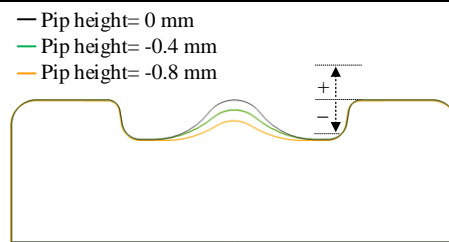


**Fig. 11** Cross-sectional profiles of the pip dies with different pip heights

## 2.2 Simulation results and discussions

For easy discussion, as shown in **Fig. 12**, three spaces in the SPR joint are defined as cavity 1 (rivet cavity), cavity 2 (die cavity) and cavity 3 (part of the die cavity underneath the rivet cavity). The relationships between the filling conditions of these cavities and the deformation behaviour of the rivet and sheets are discussed later. Two indicators as shown in **Fig. 13**, the deformed thickness at the centre of the bottom sheet ( $t_1$ ) and the flared rivet shank radius ( $R_1$ ), were also introduced to quantitatively analyse the deformations of the bottom sheet and the rivet shank.

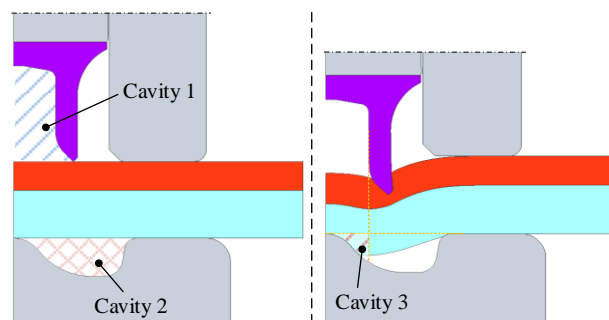


**Fig. 12** Schematic of the rivet cavity and die cavities

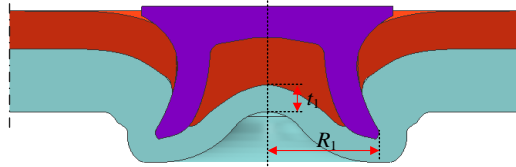


**Fig. 13** The deformed thickness at the centre of the bottom sheet ( $t_1$ ) and the flared rivet shank radius ( $R_1$ ) measured on the cross-sectional profile of SPR joint

### 2.2.1 Effect of the die type

The deformation behaviour of the rivet and sheets are closely related to the riveting force. So the force-displacement curves in joint 5-1 with the pip die P1 and joint 5-2 with the flat die F1, as shown in **Fig. 14**, were recorded to assist the study of the SPR process. A larger riveting force was observed with the pip die than that with the flat die throughout the SPR process, and the maximum value was around 10 kN larger with the pip die.

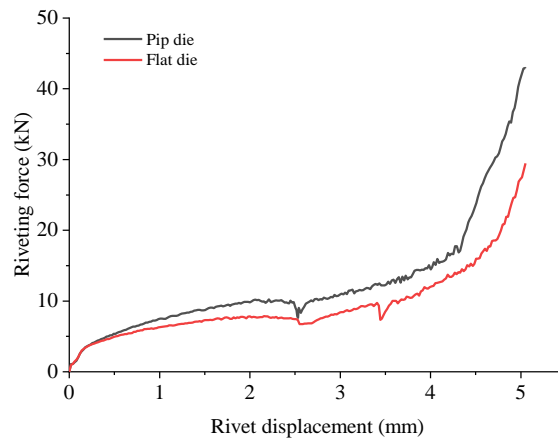


**Fig. 14** Force-displacement curves in SPR joints with the flat die F1 and pip die P1

To understand the influence of the riveting force on the rivet and sheets deformations, the cross-sectional profiles of the joint 5-1 and joint 5-2 at different rivet displacements are presented in **Fig. 15a** and **Fig. 15b** respectively. For easy explanation, the top and bottom sheets were divided into left and right parts as shown in **Fig. 15a-1**.

Different deformation behaviour of the bottom sheet with flat die and pip die were observed. Due to the existence of the die pip in joint 5-1, a resistance force was applied on the bottom of the stack at the beginning of the SPR process. A larger riveting force, as shown in **Fig. 14**, was needed for the rivet to press the sheet material into the die cavity. As a result, the bottom sheet thickness above the die pip decreased rapidly as shown in **Fig. 15a-2** to **Fig. 15a-5**, and large equivalent stresses were observed on the bottom sheet above the die pip as shown in **Fig. 16a**. Moreover, a large portion of the bottom sheet material on the left part gradually accumulated in the region where the interlock was formed. This had a positive effect on the formation of the interlock and a larger bottom sheet thickness around the rivet tip.

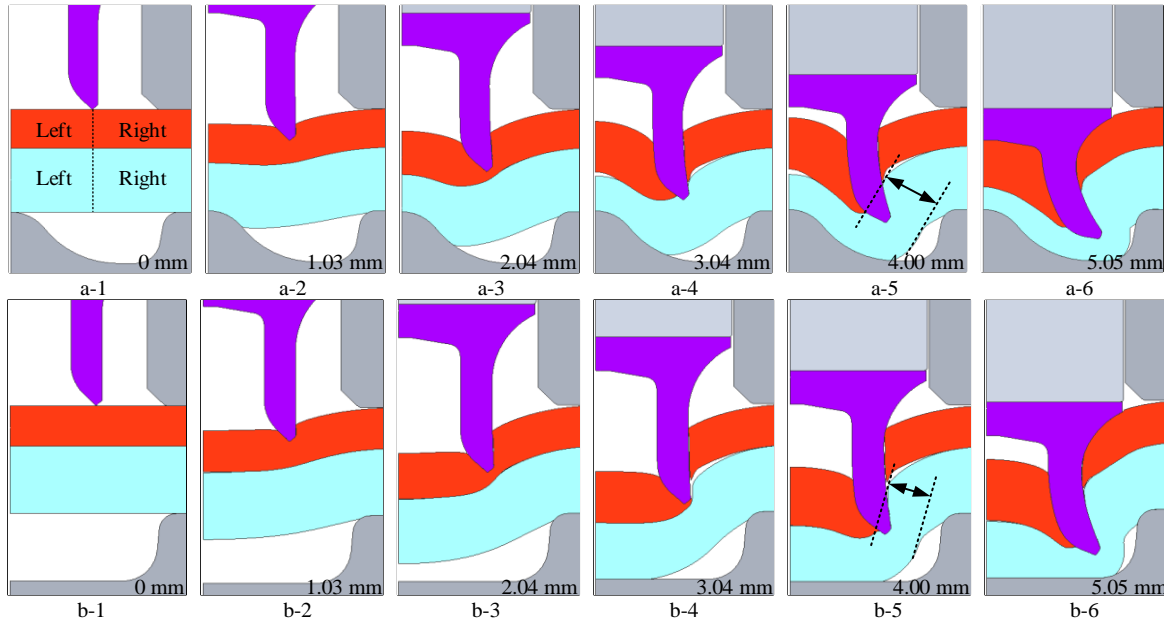


**Fig. 15** Joint cross-sectional profiles with different die types: **a** joint 5-1 with pip die P1 and **b** joint 5-2 with flat die F1

In contrast, as presented in **Fig. 15b-1**, no resistance force was applied on the bottom of the stack with the flat die at the beginning of the SPR process. As a result, the left part of the bottom sheet was rapidly pressed into the die cavity without large plastic deformation as shown in **Fig. 15b-2** and **Fig. 15b-3**. Relatively small equivalent stresses were observed on the left part of the bottom sheet as shown in **Fig. 16b**, and the bottom sheet thickness around the joint centre reduced a very small value. Furthermore, as shown in **Fig. 15b-6**, the majority of the left part material on the bottom sheet stayed underneath the rivet rather than being pressed into the region where the interlock was formed. This may have negative effects on the formation of the interlock and the final bottom sheet thickness around the rivet tip. In addition, by comparing the **Fig. 15a-6** and **Fig. 15b-6**, it can be seen that a uniformly distributed bottom sheet thickness was obtained with the pip die, while a large variation of the bottom sheet thickness was observed with the flat die. This indicated that the pip die could effectively prevent too small bottom sheet thickness in local areas, such as around the rivet tip.

For the top sheet, as presented in **Fig. 15a-5** and **Fig. 15b-5**, the left part of the top sheet with the pip die underwent a larger plastic deformation than that with the flat die. While similar deformations of the right parts of the top sheets were observed in the two joints. Therefore, the die type showed a larger effect on the bottom sheet deformation than that of the top sheet.

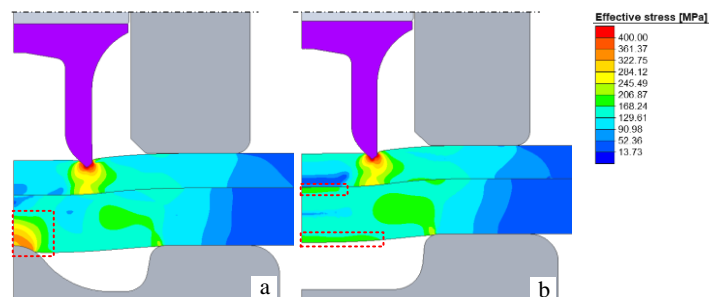


**Fig. 16** Equivalent stress distribution on the top and bottom sheets (rivet displacement=0.52mm): **a** joint 5-1 with pip die P1 and **b** joint 5-2 with flat die F1

In order to evaluate the influence of the die type on the deformation behaviour of the rivet shank, the flared rivet shank radius ( $R_1$  in **Fig. 13**) during the riveting process was recorded. **Fig. 17** and **Fig. 18** illustrate the

variation curves of the  $R_1$  with the pip die P1 and the flat die F1 respectively. According to the increasing trend, the variation curve of the  $R_1$  with the pip die was divided into two phases (I and III), while the variation curve of the  $R_1$  with the flat die was divided into three phases (I, II and III). During phase I, similar increasing patterns of  $R_1$  were observed as the rivet displacement increased: the increasing rate of the  $R_1$  firstly increased and then decreased to almost zero when the top sheets were penetrated at points  $A_1$  and  $A_2$ . This could be explained by the variation of the riveting force during this period as shown in **Fig. 14**. After the blanking of the top sheet, for the pip die, the  $R_1$  continued increasing from point  $A_1$  to the end of the SPR process (phase III). For the flat die, as shown in **Fig. 18**, the  $R_1$  kept almost constant from the point  $A_2$  to  $B_2$  (phase II), and then started increasing again at the point  $B_2$  until the end of the SPR process (phase III).

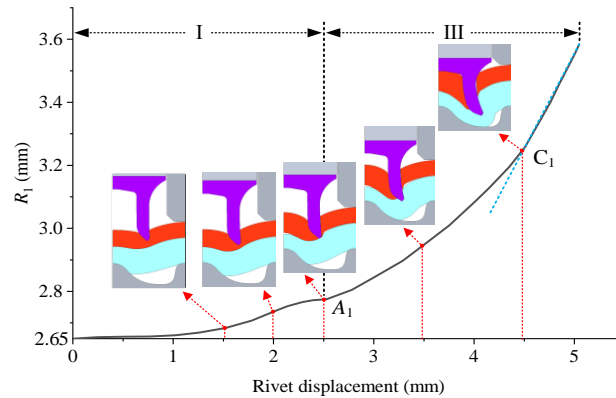


**Fig. 17** Variation curve of the flared rivet shank radius ( $R_1$ ) in joint 5-1 with the pip die P1

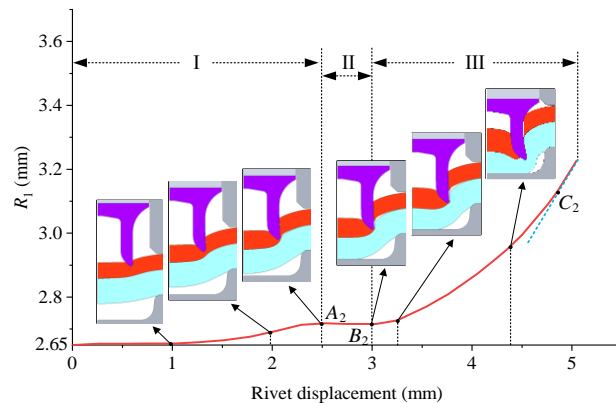


**Fig. 18** Variation curve of the flared rivet shank radius ( $R_1$ ) in joint 5-2 with the flat die F1

The major difference between the two curves is the absence of the phase II for the pip die. By observing the cross-sectional profiles of the two joints in **Fig. 17** and **Fig. 18**, it was found that the phase II depended heavily on the filling condition of the cavity 3. There was no phase II in joint 5-1 because the cavity 3 was fully filled before the top sheet was penetrated. While the phase II appeared in joint 5-2 after the top sheet was penetrated, and ended when the cavity 3 was fully filled at the point  $B_2$ . Once the cavity 3 was fully filled, the  $R_1$  started increasing rapidly (phase III).

The necessity of the fully filled cavity 3 for the rapid increase of the  $R_1$  in the phase III can be explained from different point of views. Take joint 5-2 as an example, from the point view of material flow: Before the cavity 3 was fully filled as shown in **Fig. 19a**, the bottom sheet material was pushed into the die cavity (the space in zone 1), which made more space for the top sheet material underneath the rivet shank to move downward rapidly (the material flow in zone 2). As a result, the rivet shank also moved downward rather than flaring. Therefore, the  $R_1$  kept almost constant during this period. In contrast, when the cavity 3 was fully filled as shown in **Fig. 19b**, the bottom sheet material kept being pushed into the die cavity (the space

in zone 3). However, the zone 3 is not under the rivet shank, which led to a smaller downward moving speed of the top sheet material in zone 4. Therefore, the rivet shank flared rather than moving downward, and a rapid increase of the  $R_1$  was observed. From the point view of force: As presented in **Fig. 20**, for the flat die, relatively small equivalent stresses on the rivet shank were observed after the blanking of the top sheet and before the cavity 3 was fully filled. Thus the rivet shank moved downward and the  $R_1$  kept almost constant. After the cavity 3 was fully filled, large equivalent stresses on the rivet shank were observed and the rivet shank started flaring again. So the  $R_1$  increased again with the increment of the rivet displacement.

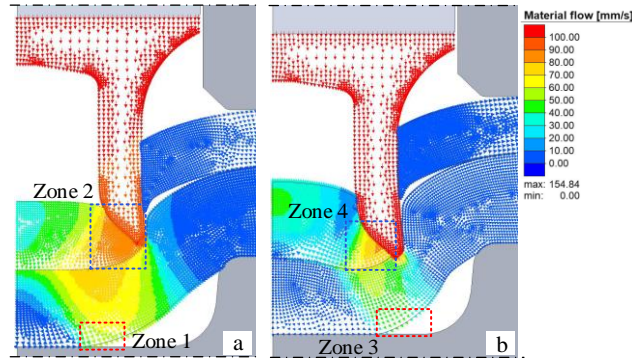


**Fig. 19** Materials flowing behaviour of the rivet and sheets in joint 5-2: **a** before and **b** after the cavity 3 was fully filled

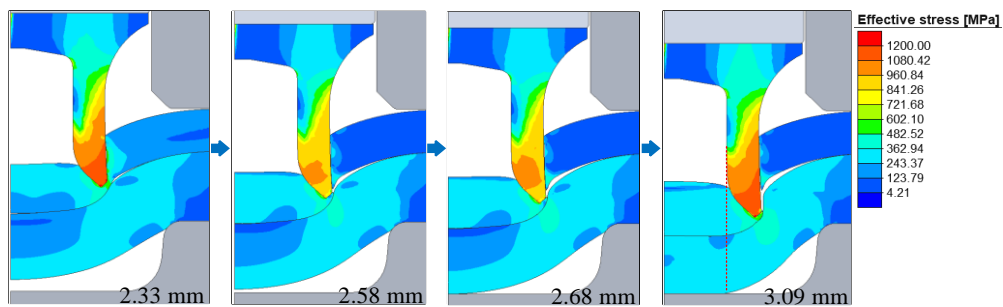


**Fig. 20** Equivalent stress distributions before and after the point *B* in joint 5-2 with the flat die F1

As shown in **Fig. 17** and **Fig. 18**, the almost linear increase of the  $R_1$  started earlier at point  $C_1$  with pip die compared with the flat die at point  $C_2$  during the phase III. This phenomenon may be related to the filling condition of the rivet cavity. In joint 5-1, the rivet cavity was gradually filled up from the point  $B_1$  to  $C_1$ . Once the rivet cavity was fully filled at the point  $C_1$ , the material within the rivet cavity showed an almost constant guidance effect on the flaring of the rivet shank. In contrast, in joint 5-2, the rivet cavity was not fully filled even at the end of the SPR process. The almost constant guidance effect appeared at point  $C_2$  when the shape of the materials underneath the rivet cavity kept almost constant.

### 2.2.2 Effect of the die diameter

The force-displacement curves of the joint 5-3, 5-4 and 5-5 with different die diameters 7.5 mm, 10.0 mm and 14.0 mm are presented in **Fig. 21**. With the increment of the die diameter, the riveting force at the beginning and at the end of the SPR process showed a decreasing trend, while it was almost same in the middle of the SPR process. Meanwhile, the maximum riveting force dropped from around 40kN to only 20kN when the die diameter changed from 7.5 mm to 14 mm.

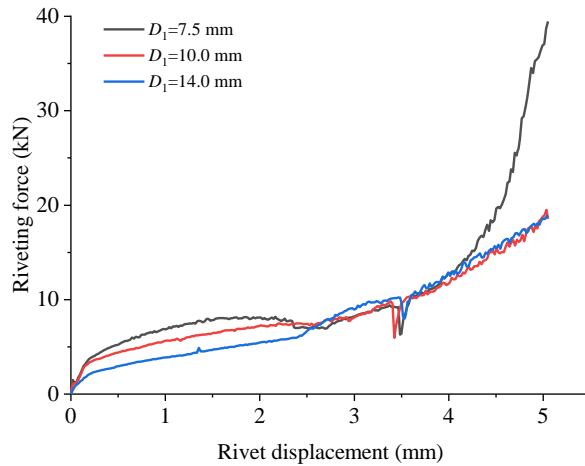


**Fig. 21** Force-displacement curves in the SPR joints with different die diameters

**Fig. 22** illustrates the cross-sectional profiles of the joint 5-3 and 5-4 at different rivet displacements. Comparing the **Fig. 22a-2~3** and **Fig. 22b-2~3**, smaller distances between the bottoms of the stack and the die cavity was observed in joint 5-4. This is because the increment of the die diameter enlarged the area of sheets above the die cavity, which made it easier for the top and bottom sheets to be bent into the die cavity and led to a slightly smaller riveting force. However, at the same rivet displacements, the depth that the rivet shank pierced into the top sheet was smaller in joint 5-4 than that in joint 5-3. This phenomenon could be explained by the relatively larger downward bending rate of the top sheet and the smaller riveting force during this period in joint 5-4 as shown in **Fig. 21**. So a larger rivet displacement was required for the rivet to penetrate the top sheet in SPR joint with a larger die diameter. Furthermore, large gaps between the rivet and the right part of the top sheet (Gap 1 and Gap 2) were observed in joint 5-4 as shown in **Fig. 22b-6**, while no apparent gap was found in joint 5-3 as shown in **Fig. 22a-6**. This was mainly attributed to the bended distance of the right part on the top sheet when the blanking of the top sheet occurred as shown in **Fig. 22a-4** and **Fig. 22b-4**. The increment of the die diameter caused a larger bended distance of the right part on the top sheet. However, the total rivet displacement was not large enough to make the rivet head to press the top sheet. So the Gap 1 and Gap 2 was not eliminated in joint 5-4 at the end of the SPR process. The appearance of these gaps may have a negative effect on the mechanical strength of the SPR joint, and they could be eliminated by using a larger rivet displacement or a smaller die diameter.

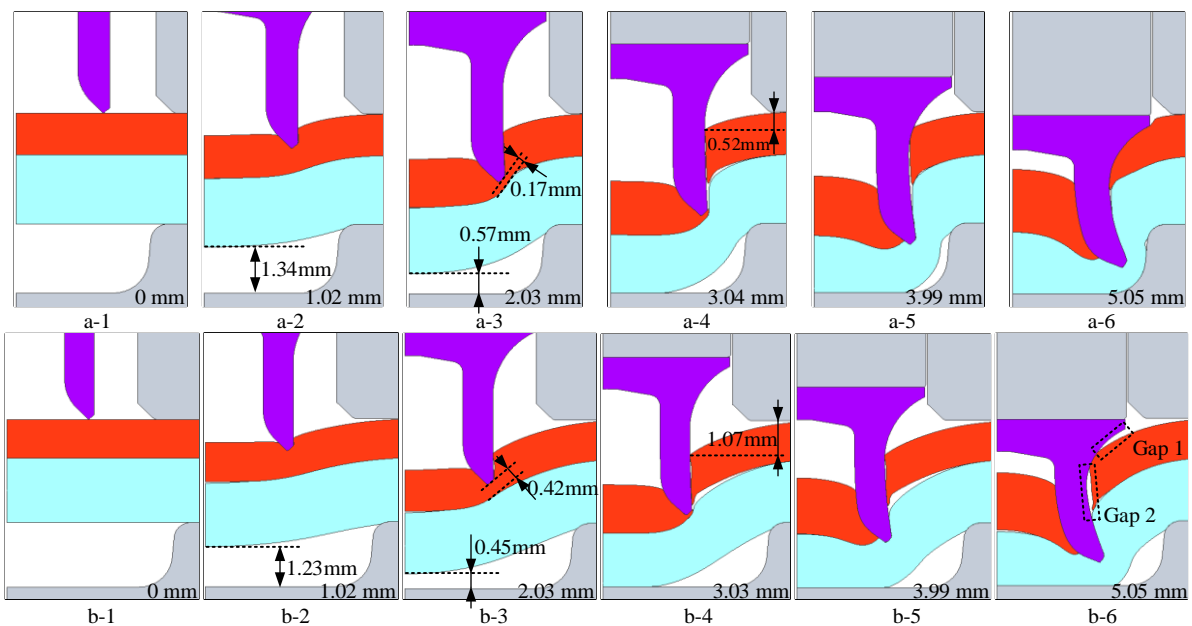


**Fig. 22** Joint cross-sectional profiles in SPR processes with different die diameters ( $D_1$ ): **a** 7.5 mm (F2) and **b** 10.0 mm (F3)

To study the influence of the die diameter on the variation of the bottom sheet thickness, the thickness at the centre of the bottom sheet ( $t_1$ ) in joints with different die diameters were recorded as shown in **Fig. 23**. For easy explanation, these curves were roughly divided into four phases according to the changing trend. Similar decreasing tendency of the  $t_1$  was observed among the three curves, except for the slight difference on the far right of these curves.

During the phase I, the left part of the bottom sheet was stretched along radial direction and large equivalent stresses were observed only on the local region around the centre of the bottom sheet as shown in **Fig. 24a**. This caused the slow decline of the  $t_1$ . Once the bottom sheet contacted with the bottom of the die cavity, large equivalent stresses were observed on a larger region around the centre of the bottom sheet as presented in **Fig. 24b**. Thus, the  $t_1$  started decreasing at a higher rate during the phase II. The phase III started when the cavity 3 was fully filled. As illustrated in **Fig. 24c**, the high stress concentration area on the bottom sheet transferred to the region around the rivet tip. The low-level equivalent stress around the centre of the bottom sheet was not large enough to cause further reduction of the  $t_1$ . Therefore, the  $t_1$  kept almost constant during this period. During the phase IV, the increment value of the  $t_1$  was heavily influenced by the filling condition of the die cavity. Take joint 5-3 as an example, the die cavity was fully filled before the end of the SPR process. With further increment of the rivet displacement, there was no space in the die cavity to accommodate extra sheet material. So the top and bottom sheets material was pressed towards the unfilled space of the rivet cavity, which caused the rapid increase of the  $t_1$ .

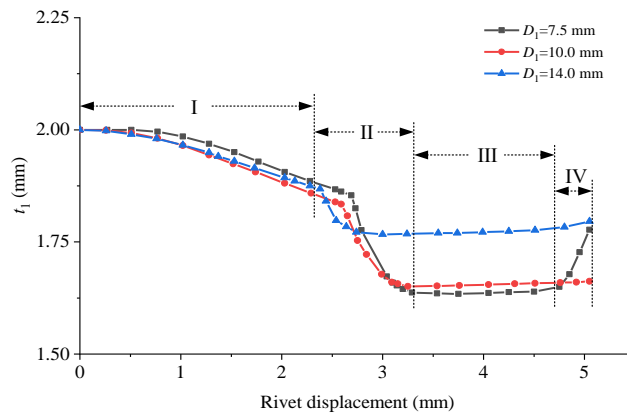


**Fig. 23** Variation curves of the thickness at the centre of bottom sheet ( $t_1$ ) in SPR processes with different die diameters ( $D_1$ )

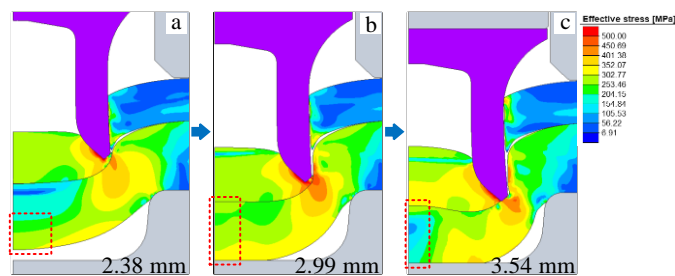


**Fig. 24** Equivalent stress distribution on the joint 5-3 in different phases (die diameter=7.5 mm): **a** phase I **b** phase II and **c** phase III

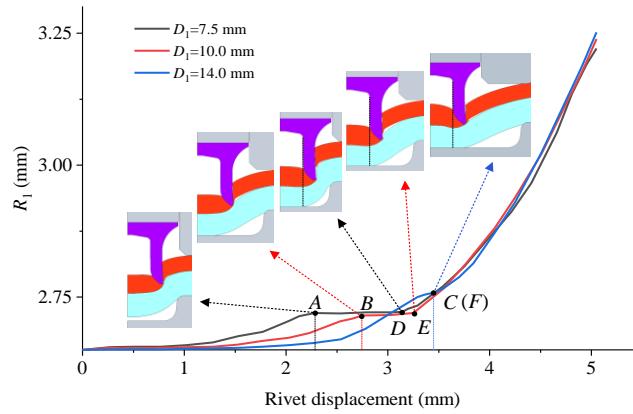


**Fig. 25** The flared rivet shank radius ( $R_1$ ) in SPR processes with different die diameters ( $D_1$ )

The variation curves of the  $R_1$  with different die diameters are illustrated in **Fig. 25**. Before the blanking of the top sheet at points *A*, *B* and *C* in different joints, a smaller increment of the  $R_1$  was observed with a larger die diameter. With the increment of the die diameter, the rivet shank encountered a smaller resistance force from the sheets as illustrated in **Fig. 21**, which caused this smaller incremental value of the  $R_1$ . After the top sheet was penetrated, the  $R_1$  kept almost constant for a period. The length of this period varied with the die diameter: the larger die diameter, the shorter this period. This is because, with a larger die diameter, the blanking of the top sheet delayed a larger time than the delayed time that the cavity 3 was fully filled. After the cavity 3 was fully filled at points *D*, *E* and *F* in different joints, a rapid increase of  $R_1$  was observed. However, very limited influence of the die diameter on the increasing rate of the  $R_1$  was observed during this period. In addition, at the end of SPR process, a little bit larger  $R_1$  was observed in joints with a larger die diameter.

From the analysis above, it was found that the die diameter had a significant influence on the rivet shank flaring behaviour. With a larger die diameter, due to the reduction of the riveting force when the rivet pierced the top sheet, it is potential to reduce the possibility of the premature rivet shank compression. Similar conclusion was also made in [9]. Although the increment of the die diameter can lead to a larger  $R_1$ , the influence of this larger  $R_1$  on the formation of the interlock need to be further investigated.

### 2.2.3 Effect of the die depth

The force-displacement curves of the joint 5-6 and 5-7 with die depth 1.8 mm and 2.4 mm are presented in **Fig. 26**. The riveting force are same on the two curves when the rivet displacement changed from 0 mm to around 2.5 mm. With further increment of the rivet displacement, a smaller riveting force was observed in joint 5-7.

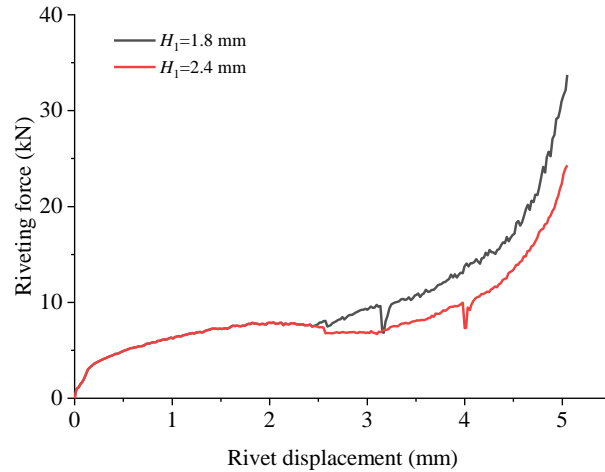


**Fig. 26** Force-displacement curves in the SPR joints with different die depths

**Fig. 27** shows the cross-sectional profiles of the joint 5-6 and 5-7 at different rivet displacements. Comparing the **Fig. 27a-1~3** and **Fig. 27b-1~3**, identical deformation behaviour of the rivet and sheets in the two joints was observed before the bottom sheet contacted with the bottom of the die cavity in joint 5-6. With a larger die depth, the bottom sheet contacted with the bottom of the die cavity at a later time in joint 5-7 than that in joint 5-6. Therefore, the bottom sheet material around the rivet tip in joint 5-7 was stretched for a longer time, which resulted in a thinner bottom sheet thickness around the rivet tip (0.79 mm) as presented in **Fig. 27b-5**. Meanwhile, it was also noted that the rivet shank did not flare into the bottom sheet when the bottom sheet thickness around the rivet tip already became very thin. This is because the cavity 3 in joint 5-7 was not fully filled for a longer period after the blanking of the top sheet. The delayed filling of the cavity 3 and the relatively smaller rivet shank flaring distance caused the smaller riveting force in joint 5-7 as shown in **Fig. 26**. This phenomenon indicated that too large die depth may have a negative effect on the formation of the interlock and the value of  $T_{min}$ .

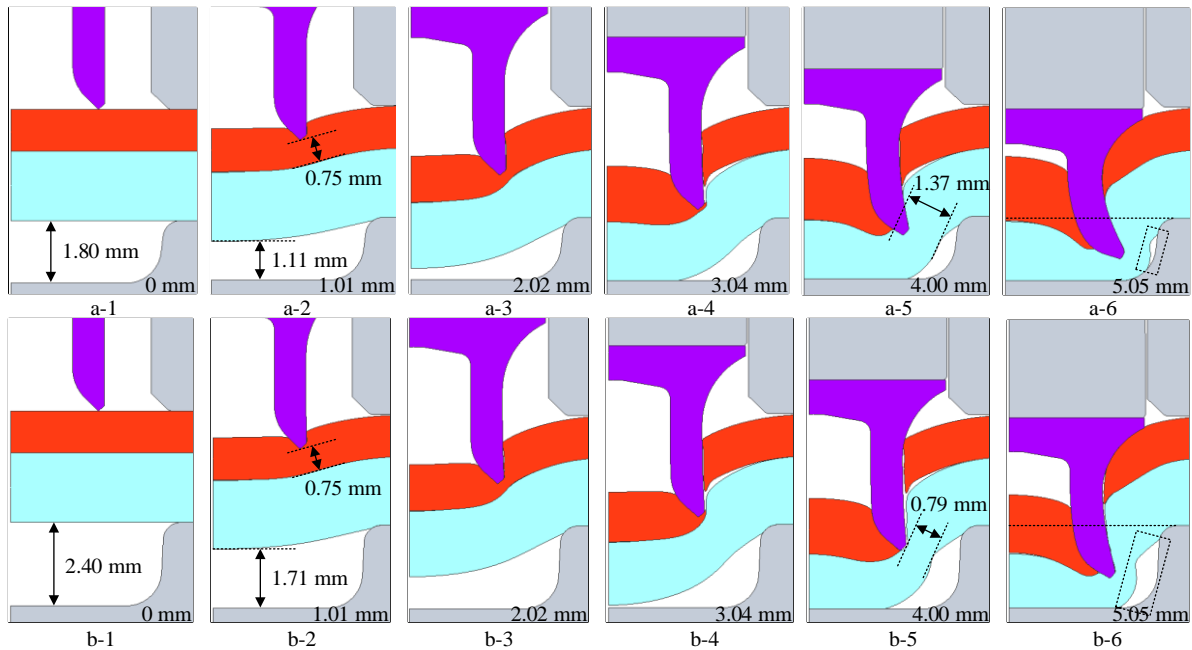


**Fig. 27** Joint cross-sectional profiles in SPR processes with different die depths: **a**  $H_1=1.8$  mm (F5) and **b**  $H_1=2.4$  mm (F6)

The variation curves of the  $t_1$  with different die depths are illustrated in **Fig. 28**. A similar changing pattern of the  $t_1$  was observed on the two curves. The values of the  $t_1$  were same on the two curves before the point

A. While the rapid decline of the  $t_1$  in joint 5-7 appeared at a later time compared with that in joint 5-6. This is caused by the delayed contact between the bottom sheet and the bottom of the die cavity in joint 5-7 at point *B*. Meanwhile, a little bit larger decreasing rate of the  $t_1$  in joint 5-7 was observed. This can be explained by the slightly larger equivalent stress distributed on the bottom sheet of joint 5-7 as shown in **Fig. 29**. Moreover, a smaller  $t_1$  was observed at the end of the SPR process in joint 5-7. So the increment of the die depth could lead to a smaller bottom sheet thickness around the joint centre.

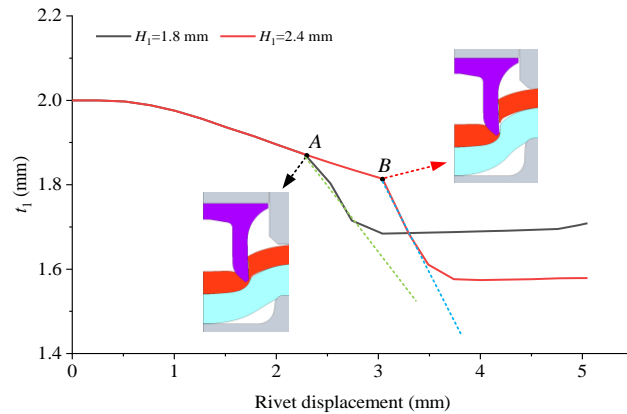


**Fig. 28** Variation curves of the thickness at the centre of bottom sheet ( $t_1$ ) in SPR processes with different die depths ( $H_1$ )

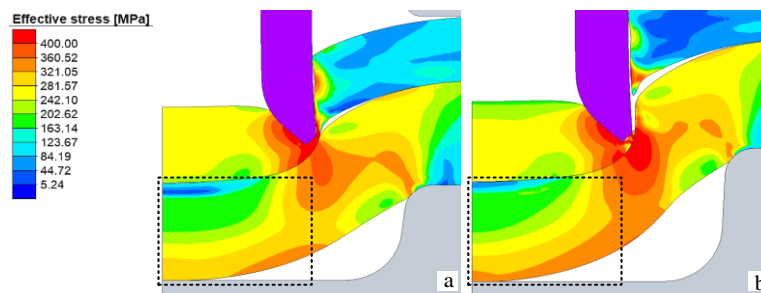


**Fig. 29** Equivalent stress distribution on the sheets after the bottom sheet contacted with the bottom of the die: **a**  $H_1=1.8$  mm (F5) and **b**  $H_1=2.4$  mm (F6)

The changing curves of the  $R_1$  with different die depths are presented in **Fig. 30**. Similarly, same increasing values of the  $R_1$  on the two curves were observed before the blanking of the top sheet at point *A*. However, the rapid increment of the  $R_1$  appeared at a later time and lasted a shorter period in joint 5-7. Almost a same increasing rate of the  $R_1$  during this rapidly increasing stage was captured. As a result, a smaller  $R_1$  was achieved in joint 5-7 at the end of the SPR process. Therefore, it can be concluded that the die depth could significantly influence the flaring behaviour of the rivet shank. Too large die depth might have a negative effect on the formation of the interlock.

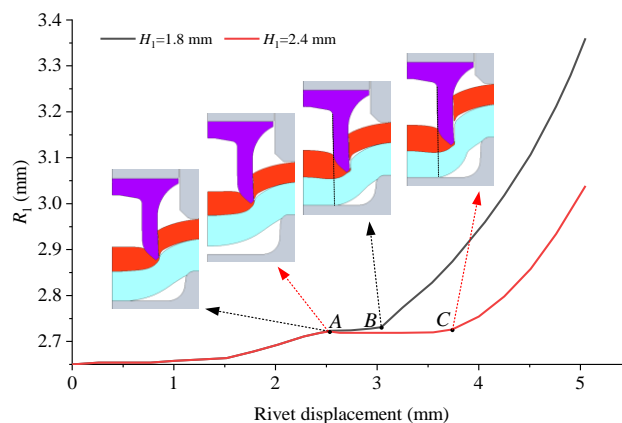


**Fig. 30** The flared rivet shank radius in SPR processes with different depths ( $H_1$ )

### 2.2.4 Effect of the die pip height

The force-displacement curves of the joint 5-8, 5-9 and 5-10 with die pip height 0 mm, -0.4 mm and -0.8 mm are presented in **Fig. 31**. With the increment of the die pip height, the riveting force at the beginning and at the end of the SPR process showed an increasing trend, while it was almost same in the middle of the SPR process. However, differing from other die parameters, no large changes of the maximum riveting force were observed.

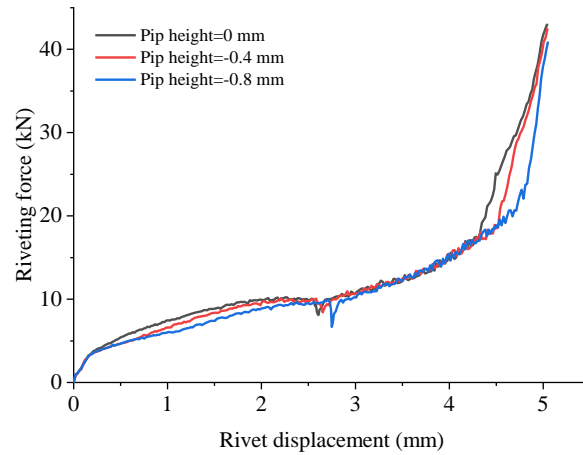


**Fig. 31** Force-displacement curves in SPR joints with different die pip heights

The cross-sectional profiles of the joint 5-8, joint 5-9 and joint 5-10 at different rivet displacements are illustrated in **Fig. 32**. Similarly to the die depth, the die pip height could directly determine the time when the die pip contacted with the bottom sheet and applied a resistance force on the bottom of the stack. As a result, the deformed bottom sheet thickness was changed as shown in **Fig. 32a-6**, **Fig. 32b-6** and **Fig. 32c-6**: the smaller the pip height, the thicker the bottom sheet thickness above the die pip. This means that the deformed bottom sheet thickness can be controlled by adjusting the die pip height. Moreover, no apparent difference of the top sheet deformation was observed.

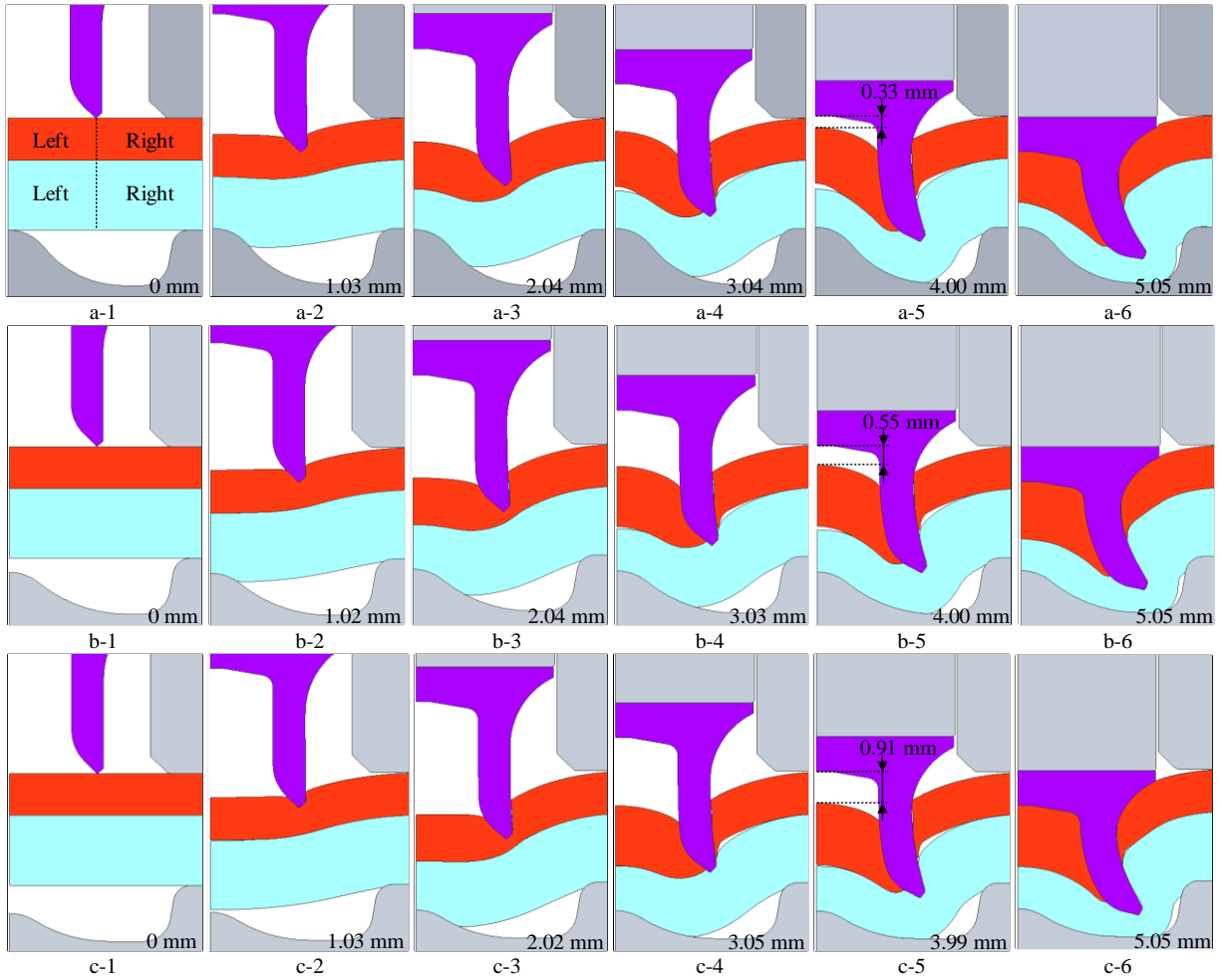


**Fig. 32** Joint cross-sectional profiles in SPR processes with different die pip heights: **a** 0 mm (P1) **b** -0.4 mm (P2) and **c** -0.8 mm (P3)

**Fig. 33** demonstrates the variation curves of the  $t_1$  with different die pip heights. When the pip height was 0 mm, the die pip contacted with the bottom of the stack at the beginning of SPR process. So the  $t_1$  decreased rapidly with the increment of the rivet displacement at the beginning of SPR process. However, when the pip height was smaller than 0 mm, the die pip did not contact with the bottom of the stack at the beginning of the SPR process. So the  $t_1$  first decreased slowly, and then decreased rapidly once the die pip contacted with the bottom of the stack. Moreover, the decreasing speed of the  $t_1$  at the end of the SPR process was almost identical among the three SPR joints, and this may be attributed to the same filling condition of the rivet cavity. This sharp decline of the  $t_1$  appeared at an earlier time and lasted a longer period with a larger die pip height. Because the rivet cavity was fully filled at an earlier time in joints with a higher die pip. In addition, it was also found that the  $t_1$  reduced a larger value not only at the beginning but also at the end of SPR process with a larger die pip height. Therefore, it can be concluded that the die pip height had a significant influence on the reduction of the  $t_1$ . The increment of the die pip height could lead to a smaller  $t_1$  at the end of the SPR process.

The variation curves of the  $R_1$  with different die pip heights are illustrated in **Fig. 34**. A similar increasing trend of the  $R_1$  was observed on the three curves. It is worth noting that the rivet shank flared a little bit larger distance at the end of SPR process with a higher die pip, and this difference was mainly formed in Zone 1

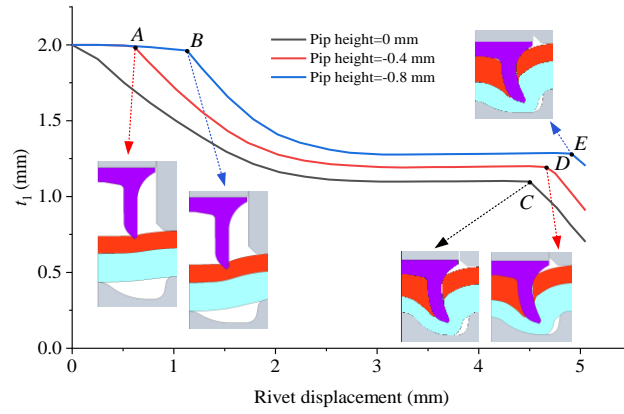


**Fig. 33** Variation curves of the thickness at the centre of bottom sheet ( $t_1$ ) in SPR processes with different die pip heights

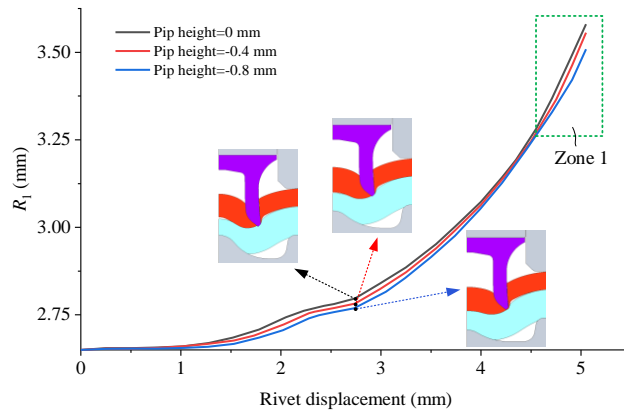


**Fig. 34** The flared rivet shank radius ( $R_1$ ) in SPR processes with different die pip heights

### 2.2.5 Interaction effects among different die parameters

In real practice, the die profile is usually optimized for a new stack configuration by changing the different parameters together. It is necessary to understand how these die parameters work together to affect the SPR process. Therefore, based on the aforementioned single die factor effects on the SPR process, the interaction effects between different die parameters were also discussed.

For the flat die, the diameter and depth are the two most important parameters. The changes of the two factors would directly affect the deformations of the rivet and sheets, and the interaction effects of them on the SPR process as well as the joint quality could be roughly estimated by the single factor effects. Roughly speaking, the single factor effects of these two parameters would be superimposed together to affect the riveting process. According to the results above, it can be concluded that the die depth had a larger influence on the SPR process and would dominate the interaction effects of these two factors. For instance, a larger die diameter (die 1) could lead to a slight increase of the  $R_1$  and  $t_1$ . For the joint quality, the interlock would decrease but the  $T_{\min}$  would show an increasing trend. In contrast, a larger die depth (die 2) could lead to an obvious decrease of the  $R_1$  and  $t_1$ . For the joint quality, both of the interlock and  $T_{\min}$  would show a decreasing tendency. If the die with a larger diameter and a larger depth (die 3), the  $R_1$  and the  $t_1$  would be more possible to reduce to a smaller value due to the dominated effect of the die depth. However, the reduction value of the  $R_1$  and  $t_1$  would be smaller than that with the die 2. For the joint quality, the interlock would reduce to a smaller value than both of the die 1 and die 2, while it is difficult to predict the  $T_{\min}$  because of the opposite changing trends caused by the larger die diameter and larger die depth.

For the pip die, except for the diameter and depth, the pip height is also a very important parameter. Although the single effects of the diameter and depth of the pip die on the SPR process were not discussed above, both

of them should have similar influences on the SPR process like that in the flat die. The interaction effects between the diameter and depth of the pip die on the SPR process would be also similar like that of the flat die. So this is not repeated again. The die with a higher pip could lead to an obvious decrease of the  $t_1$  but a slight increase of the  $R_1$ . For the joint quality, the interlock would increase with a higher die pip, but the changing trend of the  $T_{\min}$  is uncertain because of the location change. If the die with a larger diameter and a higher die pip, the  $t_1$  might lightly decrease because the die pip had a stronger effect on the  $t_1$  than the diameter, while the  $R_1$  would show an increasing trend. For the joint quality, the interlock might show a slight increase rather than decrease, while the changing trend of the  $T_{\min}$  is uncertain. If the die with a larger depth and a higher die pip, the  $t_1$  would decrease and the  $R_1$  might be also decrease because the die depth may have a larger influence than the pip height. For the joint quality, it is hard to predict the interlock and  $T_{\min}$  because of the lack of experiment or simulation data. More efforts are required to discover the interaction effects among different die parameters on the SPR process and the joint quality.

### 3 Conclusions

In this study, a 2D simulation model of the SPR joint was developed to predict the deformation behaviour of the rivet and sheets during the SPR process. The influences of the die geometric parameters on the deformation behaviour of the rivet and sheets were numerically investigated, including the die type, the diameter of flat die, the depth of flat die and the pip height of pip die. This study is benefit for the new die development and the die selection for new sheet combinations. The major conclusions are listed below:

1. Almost uniformly distributed bottom sheet thickness was obtained with the pip die, while a large variation of the bottom sheet thickness was observed with the flat die. The pip die showed a stronger guidance effect on the rivet shank flare, and has a positive effect on the formation of the interlock and a uniform deformed bottom sheet thickness.
2. The increase of the die diameter could cause a delay of the top sheet blanking, and facilitate the rivet shank flare. The thickness at the centre of bottom sheet ( $t_1$ ) first decreased and then increased with the increment of the die diameter. For a larger diameter die, a slightly larger rivet displacement should be used to eliminate the gaps between the rivet and the right part of the top sheet. This would be benefit for the improvement of the joint mechanical strength.
3. The increment of the die depth could cause a reduction of the flared rivet shank radius ( $R_1$ ), which had a negative effect on the joint quality, mainly on the interlock. It could also lead to a reduction of the  $t_1$  and a smaller bottom sheet thickness around the rivet tip.
4. The increment of the die pip height could lead to a smaller  $t_1$  but a larger  $R_1$ . By adjusting the die pip height, the thickness distribution on deformed bottom sheet can be controlled to improve the joint quality.
5. Moreover, it was found that the flaring behaviour of the rivet shank depended heavily on the filling condition of the die cavity underneath the rivet cavity (cavity 3). Rapidly rivet shank flare was observed once the cavity 3 was fully filled.

### Acknowledgements

The authors gratefully acknowledge Jaguar Land Rover for sponsoring this project.

### References

1. Han L, Thornton M, Shergold M (2010) A comparison of the mechanical behaviour of self-piercing riveted and resistance spot welded aluminium sheets for the automotive industry. *Mater Des* 31:1457–1467

2. Huang Z, Yao Q, Lai J, Zhao J, Jiang Z (2017) Developing a self-piercing riveting with flange pipe rivet joining aluminum sheets. *Int J Adv Manuf Technol* 91:2315–2328
3. Kochan A (2000) Audi moves forward with all-aluminium cars. *Assem Autom* 20:132–135
4. Mortimer J (2001) Jaguar uses X350 car to pioneer use of self-piercing rivets. *Ind Robot An Int J* 28:192–198
5. Li D, Chrysanthou A, Patel I, Williams G (2017) Self-piercing riveting-a review. *Int J Adv Manuf Technol* 92:1777–1824
6. He X, Xing B, Zeng K, Gu F, Ball A (2013) Numerical and experimental investigations of self-piercing riveting. *Int J Adv Manuf Technol* 69:715–721
7. Li D, Han L, Lu Z, Thornton M, Shergold M (2012) Influence of die profiles and cracks on joint buttons on the joint quality and mechanical strengths of high strength aluminium alloy joint. *Adv Mater Res* 548:398–405
8. Ma Y, Lou M, Li Y, Lin Z (2018) Effect of rivet and die on self-piercing rivetability of AA6061-T6 and mild steel CR4 of different gauges. *J Mater Process Technol* 251:282–294
9. Mori K, Abe Y, Kato T (2007) Finite element simulation of plastic joining processes of steel and aluminum alloy sheets. *AIP Conf Proc* 908:197–202
10. Abe Y, Kato T, Mori K (2008) Self-pierce riveting of three high strength steel and aluminium alloy sheets. *Int J Mater Form* 1:1271–1274
11. Jäckel M, Falk T, Landgrebe D (2016) Concept for Further Development of Self-pierce Riveting by Using Cyber Physical Systems. *Procedia CIRP* 44:293–297
12. Drossel WG, Jäckel M (2014) New Die Concept for Self-Pierce Riveting Materials with Limited Ductility. *Key Eng Mater* 611:1452–1459
13. Landgrebe D, Jackel M, Niegsch R (2015) Influence of Process Induced Damages on Joint Strength when Self-Pierce Riveting Carbon Fiber Reinforced Plastics with Aluminum. *Key Eng Mater* 651:1493–1498
14. Hoang NH, Porcaro R, Langseth M, Hanssen AG (2010) Self-piercing riveting connections using aluminium rivets. *Int J Solids Struct* 47:427–439
15. Porcaro R, Hanssen AG, Langseth M, Aalberg A (2006) Self-piercing riveting process: An experimental and numerical investigation. *J Mater Process Technol* 171:10–20
16. Carandente M (2016) FE simulation of the SPR process to predict joint characteristics: innovation report. University of Warwick
17. Carandente M, Dashwood RJ, Masters IG, Han L (2016) Improvements in numerical simulation of the SPR process using a thermo-mechanical finite element analysis. *J Mater Process Technol* 236:148–161
18. Han SL, Tang XD, Gao Y, Zeng QL (2015) Effects of friction factors on flat bottom self-pierce riveting joints of AZ31 magnesium alloy. *Mater Res Innov* 19:S10-235
19. Hoang N-H, Hopperstad OS, Langseth M, Westermann I (2013) Failure of aluminium self-piercing rivets: An experimental and numerical study. *Mater Des* 49:323–335
20. Mucha J (2011) A study of quality parameters and behaviour of self-piercing riveted aluminium sheets with different joining conditions. *Stroj Vestnik/Journal Mech Eng* 57:323–333
21. Han L, Hewitt R, Shergold M, Chrysanthou A, Stepinski T (2007) An evaluation of NDT for self-pierce riveting. *SAE Tech Pap.* doi: 10.4271/2007-01-1364